THE ASTROPHYSICAL JOURNAL, 456:194–205, 1996 January 1

STELLAR KINEMATICS AND THE BLACK HOLE IN THE GALACTIC CENTER[1]

JOSEPH W. HALLER, M. J. RIEKE,[2] G. H. RIEKE,[2] P. TAMBLYN, L. CLOSE, AND F. MELIA
Steward Observatory, University of Arizona Tucson, AZ 85721
Received 1995 May 4; accepted 1995 July 10

ABSTRACT

We estimate the amount and distribution of matter in the Galactic center, based on measurements of stellar velocities. In addition to published data, we consider new observations of the CO ($v = 2 \leftarrow 0$) 2.3 μm absorption feature in the unresolved stellar emission at 41 positions within 20″ of Sgr A*. Because the CO band strength is greatly reduced within 6″–8″ of Sgr A*, we model the three-dimensional distribution of the stars with this feature. We find that the CO-bearing stars can provide a useful lower limit to the enclosed mass. We also analyze the velocities of the He I–emitting stars within 20″ of Sgr A*. We find a correlation between the He I line width and the radial velocity of these stars, indicating that the velocity dispersion derived from the He I stars is an upper limit to the intrinsic value, and hence the corresponding enclosed mass is an upper limit. Because this upper limit and the lower limits derived from the CO-bearing stars are virtually the same, at just under $2 \times 10^6\ M_\odot$, we conclude that the stellar dynamics require a concentrated central mass of this amount. This value is in close agreement with the mass deduced from gas velocities measured with the [Ne II] line. Although it is most likely that this central mass is in the form of a black hole, we cannot exclude the possibility of a tightly concentrated cluster of stellar remnants. In addition, we infer the possible existence of an extended component of dark matter, which might also be attributed to stellar remnants.

Subject headings: black hole physics — Galaxy: center — Galaxy: kinematics and dynamics

1. INTRODUCTION

The mass distribution at the Galactic center, specifically whether the Milky Way has a central massive black hole, is critical to understanding the processes occurring there and placing them among the phenomena seen in much less detail in other galactic nuclei. Two types of probe have been employed to determine the mass: (1) the motions of gas clouds and streamers (e.g., Lacy et al. 1980; Genzel & Townes 1987; Lacy 1989; Lacy, Achtermann, & Serabyn 1991); and (2) the dynamics of stars (e.g., Sellgren et al. 1987; Rieke & Rieke 1988; McGinn et al. 1989; Sellgren et al. 1990; Lindqvist, Habing, & Winnberg 1992). Each method is subject to biases and possible systematic errors. The gas motions may be influenced by nongravitational forces, particularly in the crucial innermost few tenths of a parsec. Interpreting the dynamics of the stars depends on knowledge of their orbital parameters and of their distribution around the possible black hole. Fortunately, the two approaches give consistent results, implying the existence of a central mass of $2–5 \times 10^6\ M_\odot$. Unfortunately, this result never seems to be established at better than a 3 or 4 standard deviation level of confidence, even if only the nominal errors are considered. Since the possible systematic errors can reduce the significance of the central mass determination below even these modest values, to be confident would require either a far stronger case for a central mass with one method or that two methods subject to different systematic effects provide results in close agreement.

In this paper, we reconsider the determination of the mass using stellar dynamics. We assume a distance to the Galactic center of 8.5 kpc. We will consider the velocities of the faint unresolved stellar emission (McGinn et al. 1989; Sellgren et al. 1990) both by adding an extensive set of measurements very close to Sgr A* and by improving models of the distribution of CO-bearing stars in the central parsec. We will reconsider measurements of velocities of individual bright stars within the central 10 pc radius (Sellgren et al. 1987; Rieke & Rieke 1988). We will also present velocity measurements of the very compact cluster of He I stars around Sgr A* and will use them to complement the information available from the cool stellar population studied with the CO band head.

These data will be integrated with mass determinations on a larger scale, primarily from the OH/IR measurements of Lindqvist et al. (1992). With the improved data and modeling of the stellar populations, we can derive a more reliable mass distribution than has been possible previously. We show that the stellar dynamics give results closely in agreement with the mass derived from gas motions.

2. NEW OBSERVATIONS

Spectra of the He I line in warm Galactic center stars were obtained on 1994 April 28 and 30, May 1, June 26, and July 2 (U.T.). The Multiple Mirror Telescope was used in April and May and the Steward Observatory Bok 2.3 m Telescope in June and July. The same spectrometer (Williams et al. 1993) was employed at both telescopes, using a NICMOS3 256 × 256 detector array and giving a per-pixel resolution of ~7000, or 43 km s^{-1}. At the MMT, the pixels project to 0.″4, the slit is 1.″2 × 32″, and the seeing for these measurements was ~1″. The achieved resolution determined from the FWHM of night sky lines is ~2250. At the 2.3 m the pixels project to 1.″2, the slit is 2.″4 × 96″, and the seeing was 1.″5. The achieved spectral resolution is ~2500. Details of these measurements and their reduction are provided by Tamblyn et al. (1996).

The CO-band spectra presented here were taken at the CTIO 4 m telescope using the facility Infrared Spectrometer on

[1] Some of our observations made use of the Multiple Mirror Telescope, operated jointly by the Smithsonian Astrophysical Observatory and Steward Observatory.

[2] Guest Observer, Cerro Tololo Inter-American Observatory.

TABLE 1

2.3 μm SPECTRA SLIT POSITIONS

Night of Observations (1989)	Slit Position	$\alpha_{IRS\ 7}$	$\delta_{IRS\ 7}$	Total Exposure Time (s)
Jun 24/25.....	1	−1.″5	−8.″0	1200
	2	−3.5	−7.0	480
	3	+3.5	−7.0	480
Jun 26/27.....	5	−4.0	+3.0	480
	6	−9.0	−18.0	480
	7	+0.0	+11.0	240
Jun 28/29.....	8	+5.5	−4.5	480
	9	+0.0	−14.5	480
	WI16	−1.5	−8.0	240

the nights of 1989 June 25, 27, and 29 (U.T.). The detector was a SBRC 58 × 62 InSb array. The spatial scale along the slit was 0.″81 pixel^{-1}, and the grating was set for a per-pixel resolution of ~3000, with a corresponding velocity resolution of 100 km s^{-1}. The slit was 15″ × 1.″3 in projected size on the sky, oriented in the north-south direction. Table 1 lists the nominal slit coordinates offset from IRS 7 and the cumulative exposure times. At each slit position, spectra were taken at the nominal wavelength of 2.3 μm as well as with the grating "jogged" by 0.5 of a pixel element so the light was sampled at twice the pixel resolution. The slit was placed by peaking the signal on IRS 7 and then offsetting the telescope to the desired position (see Fig. 1); correct positioning was verified by comparing the pattern of continuum emission along the slit with a high-resolution image. For sky subtraction, frames at the same exposure were obtained from a position ~90″ south of the nominal slit position in a region of strong interstellar obscuration.

Images of the Galactic center were obtained at K_s (2.0–2.3 μm) and through a narrowband filter in the CO absorption band ($\lambda_0 = 2.34$ μm, $\Delta\lambda = 0.07$ μm) on the Bok Telescope on 1993 June 1. The FASTTRAC tip-tilt secondary mirror (Close & McCarthy 1994) was used to compensate image motion; IRS 7 was used as an infrared guide star. The heavily absorbed area to the east was used as a flat field. The resolution achieved with these data is 0.″5 FWHM at K_s and 0.″6 at CO.

A large-scale image at K(2.2 μm) was acquired on 1992 May 11, using a 256 × 256 NICMOS3 camera (Rieke et al. 1993) on the Steward 2.3 m telescope. A plate scale of 0.″64 pixel^{-1} was used to give a total field of view of 164″ × 164″ for one image; the seeing was 1.″6 FWHM. The observations for each frame were obtained as a 4 × 4 grid of 3 s exposures spaced on 5″ centers. A 3 × 3 mosaic of frames was obtained (except for the southeastern corner of the grid), centered on IRS 7. The positions were spaced to give an overlap of 25″ in each coordinate. A sky reference for flat-fielding was obtained at a similar elevation but at 1^h earlier in right ascension.

3. DATA REDUCTION

The CTIO spectra were reduced along similar lines to the MMT and Bok data (Tamblyn et al. 1996). After subtracting sky, the spectra were divided by dark current–corrected dome flats. Atmospheric absorptions were corrected by dividing by a spectral reference observation of a G dwarf star, obtained at the same air mass and shortly before or after the Galactic center observation. Eighteen spectra were extracted from each

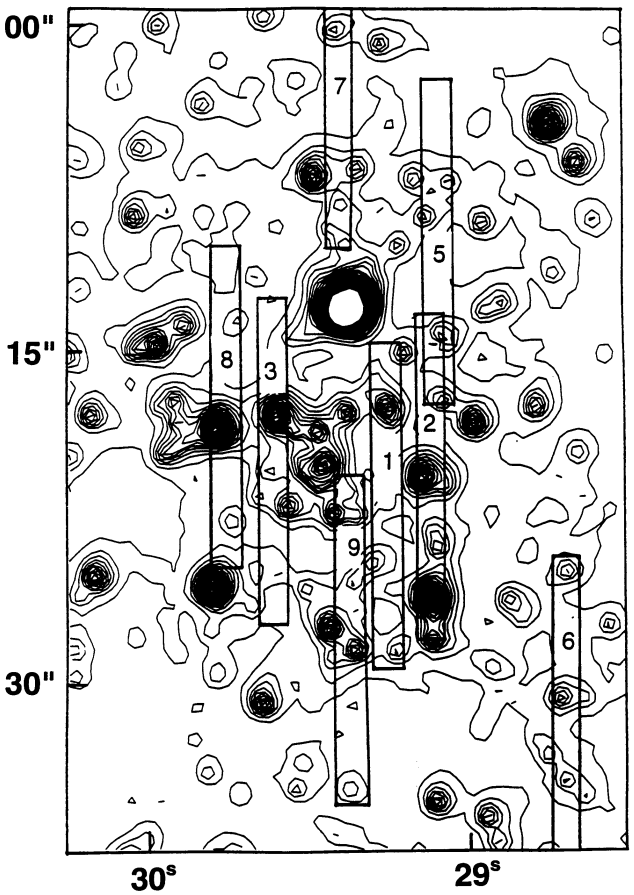

FIG. 1.—Slit positions for measurements of diffuse CO emission

slit position, 2 pixels wide in the spatial direction with an effective beam size of $\Delta\alpha \times \Delta\delta = 1.''3 \times 1.''6$ and sequentially spaced by 1 pixel from north to south. The extracted spectra were normalized to unity in the continuum blueward of the 2.29 μm CO absorption feature. The final spectra had a velocity width of 4700 km s^{-1} with an inverse dispersion of 49 km s^{-1} pixel^{-1}.

A 0.″5 resolution K_s band (2.0–2.3 μm) image was cleaned of all point sources by DAOPHOT to produce a continuum map. A similarly cleaned CO image (of 0.″6 resolution) was also prepared. The two images in and out of the CO band were adjusted in normalization and offset until the majority of diffuse emission outside the central 10″ radius disappeared in the ratio of the images. With these adjustments, a star with a CO absorption strength typical of the red giants in the Galactic center will not be prominent in the ratioed image, but stars with reduced CO absorption will stand out clearly. The resulting extinction-independent image of the diffuse emission in the CO band is shown in Figure 2. In this figure, the region to the north of Sgr A* is occulted by the guide probe used to deliver the image of IRS 7 to the rapid guide camera.

The 16 data frames for each position in the large-scale K image were median combined. The images were reduced and mosaicked using IRAF routines, and the actual sky level in the final image was estimated from the flux levels seen from regions with the heaviest extinctions. Fluxes were calibrated by assuming that the brightest sources as listed in Rieke, Rieke, & Paul (1989) had not varied. The final image was trimmed to 330″ × 330″.

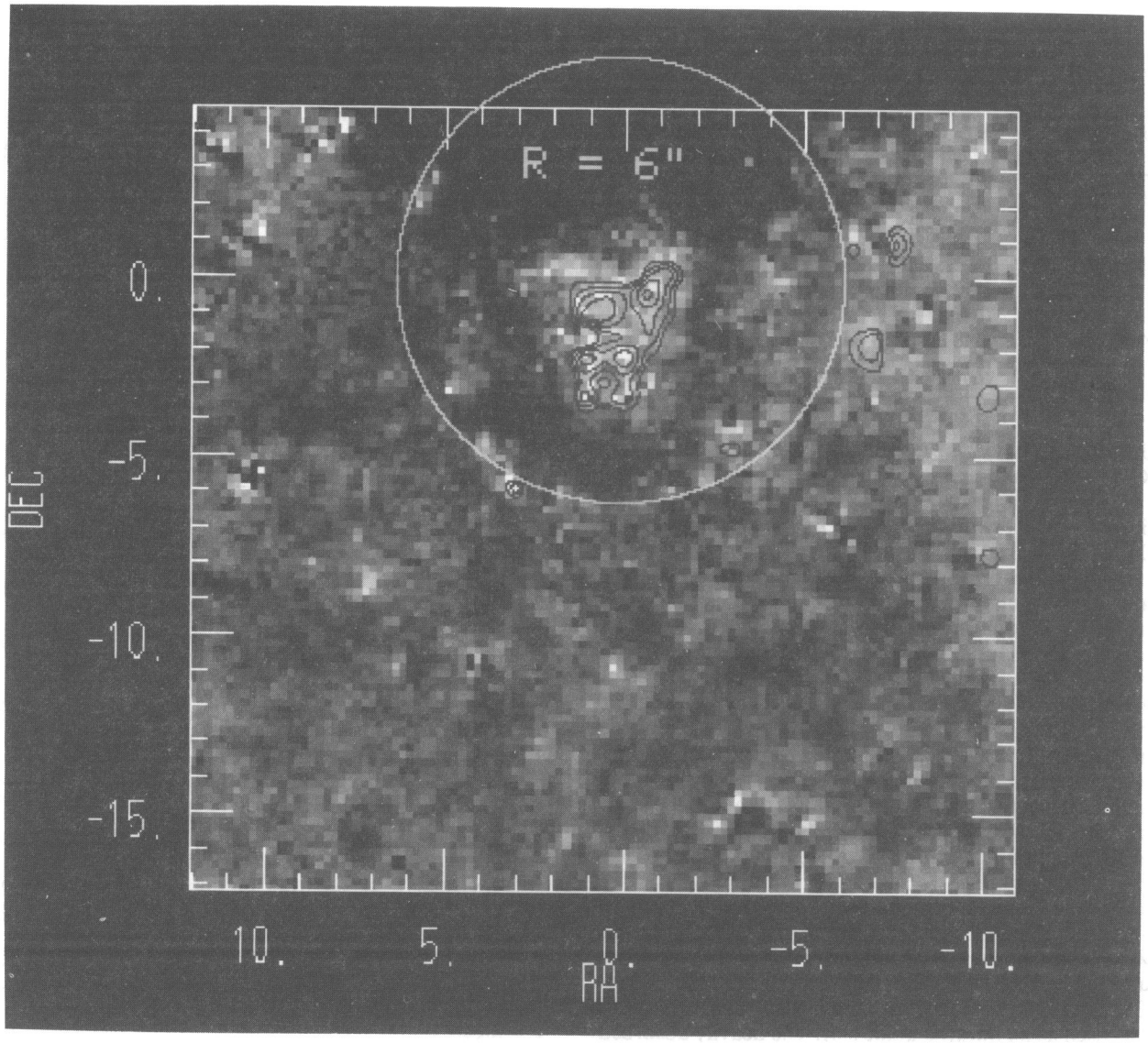

FIG. 2.—Image of the diffuse emission in the CO filter. The bright emission centered on Sgr A* (location 0″, 0″) indicates a reduction in the CO band head absorption strength within 6″ of Sgr A*. The dark patch above Sgr A* is an artifact produced by the shadow of FASTTRAC's pick-off mirror. The contour lines have been smoothed by 3 × 3 block-averaging and are at the 6, 7.5, 9, and 10.5 smoothed sigma level.

4. LINE-OF-SIGHT VELOCITIES AND VELOCITY DISPERSIONS

4.1. *Individual* He I *Stars*

Unlike the predominantly diffuse hydrogen recombination lines, He I emission images by Allen et al. (1989) and Krabbe et al. (1991) indicate that much of the He I emission is associated with individual stars. Recent higher resolution images (Rieke & Rieke 1994; Tamblyn et al. 1996) further resolve the He I emission from the IRS 16 complex and tie it to the dominant stellar components, while confirming that the Brγ is largely diffuse in nature. Therefore, the He I velocities centered on individual stars should represent the velocities of this stellar population. The initial spectra of the IRS 16 region showed very broad He I emission (Hall, Kleinmann, & Scoville 1982; Wollman, Smith, & Larson 1982), suggesting wind velocities as high as 1000 km s^{-1}. The relatively high spatial resolution of our spectra (Tamblyn et al. 1996) shows that, in some cases, the apparently broad lines resulted from the superposition of a number of these stars with different velocities and that the population of hot stars includes a number with relatively narrow lines.

The velocities of the He I stars were measured by selecting pointlike objects in the continuum that have significantly stronger He I than the surrounding region, fitting Gaussians to their He I line profiles, and comparing the position of each Gaussian to the wavelengths of the OH airglow lines, which are numerous and strong in this part of the spectrum. Similar spectra are illustrated in Tamblyn et al. (1996). The resulting velocities are entered in Table 2. For the complete sample, there is a significant correlation between line width and the absolute value of V_{LSR}, as might be expected if vigorous stellar winds and complex line profiles and the resulting measurement errors contribute to the apparent velocity shifts. Therefore, masses computed from He I star velocities, particularly if stars with relatively broad lines are included, should be interpreted as upper limits. To minimize this bias, we will use as mass

TABLE 2

He I VELOCITIES

Source	$\Delta\alpha$[a]	$\Delta\delta$[a]	r[a]	FWHM (km s^{-1})	v_{lsr} (km s^{-1})
16NW1	−1″	1″	1″	180	−196
16NW2[b]	−1	1	1	320	433
29[b]	−2	1	3	250	−194
16NE	3	1	3	170	34
GCHe5[c]	−3	3	4	150	−26
GCHe3[c]	−2	−5	5	120	−239
13[b]	−4	−2	5	210	−153
34[b]	−5	1	5	230	−174
Between 10E, 16NE	8	5	5	150	34
GCHe2[b,c]	4	−7	8	220	180
E of 9	7	−8	10	150	132
5	9	10	13	150	85
E of 11	−10	12	16	180	−18

[a] Positional offsets from Sgr A*.
[b] Line FWHM > 200 km s^{-1}.
[c] See Tamblyn et al. 1996 for nomenclature.

probes only individual stars in which the He I line width is <200 km s^{-1} FWHM, but we will show that our results are not strongly dependent on this selection criterion. For these stars, ambiguities in the fitted velocities should be well under the intrinsic velocity dispersion for this population.

4.2. *Diffuse Emission*

The CO absorption bands in the diffuse emission were analyzed using the velocity standard exposures of IRS 7 as templates for measuring the radial velocity and velocity dispersion. Each spectrum of IRS 7 was convolved with Gaussian functions corresponding to a range of velocity dispersions from 0 to 300 km s^{-1}. The data and the velocity standards were linearly interpolated to 4 times the pixel resolution, renormalized to the CO band depth of the velocity standard, and cross-correlated. The velocity dispersion, σ_{RAW}, and offset velocity from IRS 7, $V_{IRS\,7}$, were determined by finding the minimum of the $\chi^2(v)$ curves in the σ_{RAW}-$V_{IRS\,7}$ plane by parabolic interpolation. The slit positions and measured values of σ_{RAW}, and $V_{IRS\,7}$ values are shown in Table 3.

Error analysis was done by Monte Carlo simulation. In general it was found that successful cross-correlation systematically overestimated $\langle\sigma_v\rangle$ and $\langle V_{IRS\,7}\rangle$ with errors that monotonically decreased with increasing signal-to-noise ratio (S/N). Below a S/N of 10, the measured value of $\langle\sigma_v\rangle$ was $\sim$190 km s^{-1} independent of the intrinsic velocity dispersion, while for S/N > 40 the fractional error of σ_v was independent of the true velocity dispersion. The measured systematic velocity with respect to the template spectrum was always on the order of a few km s^{-1} with an error on the order of 5 km s^{-1} for S/N > 20 and was not a strong function of intrinsic velocity dispersion. The yield rate of the cross-correlation program was also an increasing function of S/N. At fixed S/N, the yield rate decreased significantly for $\sigma_v(0)$ greater than 100 km s^{-1}.

TABLE 3

RAW VELOCITY DISPERSIONS AND RELATIVE VELOCITIES FROM IRS 7

Slit Position	S/N	θ_{SGRA*}	σ_{RAW} (km s^{-1})	$V_{IRS\,7}$ (km s^{-1})
P1 − 11[a]	48	5″.2	142.5	+41.0
P1 − 12[a]	61	6.4	98.5	+29.8
P1 − 13[a]	51	6.9	101.2	+60.7
P1 − 14	44	7.7	111.3	+77.7
P1 − 15	43	8.6	112.3	+80.3
P1 − 17	22	10.3	108.6	+127.8

[a] Radial distance from Sgr A* < 7″.

Six spectra from slit Position 1 (Fig. 1) had sufficient S/N to produce good cross-correlations for velocity measurements and reliable systematic error corrections. Table 4 lists the corrected velocity dispersions, V_{LSR} velocities, and estimated errors for the measurements listed in Table 3. The column listing ΔV_{LSR} gives the systematic error correction and dispersion, respectively. The nominal V_{LSR} of IRS 7 was taken to be −130 km s^{-1} (Sellgren et al. 1987).

The Monte Carlo simulations demonstrated that the computer extractions favored spectra with small dispersions and hence might bias our results. We therefore inspected the spectra carefully to locate all regions with velocity dispersions greater than $\sim$100 km s^{-1} that had been missed by the computer. For these regions, we fitted the suite of template curves by eye. As a check, these fits were carried out by one of us and then rated for acceptance by a second. It is not possible to analyze the errors in these fits systematically as with the computer extractions. Fortunately, since the dispersions are relatively high, the fractional errors of measurement should tend to be modest. The additional velocities and dispersions are listed in Table 5.

5. THE CO ABSORPTION FEATURE AND ITS INTERPRETATION

In modeling the mass distribution from the CO band head, it is important to understand the physical location of the CO-bearing stars. Allen et al. (1989) and Sellgren et al. (1990, hereafter SMBH) both noticed a reduction in CO strength in the region immediately surrounding Sgr A*. SMBH concluded that any CO bands measured close to Sgr A* are likely to be from stars that lie significantly in front of or behind Sgr A* and that appear to be close to Sgr A* only in projection. If not correctly modeled, such a geometry would result in an underestimate of the enclosed mass.

To analyze our data for this effect, we define the CO band strength as the depth of the absorption feature immediately to the red of the band head relative to the blueward continuum. Point sources identified on the high-resolution image were excluded from the CO sample. The CO band strength is at least partially diluted by broadening due to the high velocity dispersion. The resulting fractional change in CO strength was computed from the IRS 7 template spectra for the range of the measured velocity dispersions and was found to be 15%–20%. A nominal correction of 20% was applied for the purpose of comparing to our models. The derived CO depth versus angular distance from Sgr A* is shown in Figure 3. We confirm the result of the earlier studies that CO absorption is diminished within an $\sim$8″ (0.33 pc at a distance of 8.5 kpc) radius from Sgr A*. The dispersion of the correlation is insensitive to recentering within $\pm$1″.0 of Sgr A*. We find that the average band strength outside a radius of 20″ is $\sim$35%, in agreement with SMBH. However, in the 10″ < r < 20″ region the strength is $\sim$27%, substantially higher than found by them; the difference probably results from the larger number of measurements in our study. The small dimunition of the CO band in this intermediate zone suggests that the band disappears relatively sharply near a radius of 6″–10″.

TABLE 4

CORRECTED VELOCITY DISPERSIONS AND LINE-OF-SIGHT VELOCITIES

Slit Position	S/N	β[a]	$\Delta\beta$[b]	$\Delta\sigma_{RAW}$ (km s^{-1})	ΔV_{LSR} (km s^{-1})	σ_v (km s^{-1})	V_{LSR} (km s^{-1})
P1 – 11[c]	48	0.13	0.05	21	−4.5/7	126 ± 19	−93 ± 7
P1 – 12[c]	62	0.08	0.02	15	−2.8/6	91 ± 15	−103 ± 6
P1 – 13[c]	52	0.11	0.03	17	−3.7/7	91 ± 17	−66 ± 7
P1 – 14	45	0.12	0.06	19	−4.3/8	99 ± 18	−56 ± 8
P1 – 15	44	0.12	0.06	19	−4.3/8	100 ± 18	−54 ± 8
P1 – 17	22	0.45	0.50	38	−14.4/7	75 ± 37	−16 ± 17

[a] Fractional systematic error in the derived velocity dispersion, as determined by Monte Carlo simulation.

[b] Dispersion in the values of β in the simulation.

[c] Radial distance from Sgr A* < 7″.

SMBH presented models of the Galactic center unresolved population to interpret the CO depletion. At large radii, the 2.2 μm light distribution depends on radius as $R^{-0.8}$ (Becklin & Neugebauer 1968; see § 6), which implies a stellar number density that goes as $R^{-1.8}$. The core radius of this distribution is approximately 3″.8 (Eckart et al. 1993). The luminosity density of 2.2 μm sources can be represented by

$$F_K(r) = F_K(0) \; ; \qquad r \le R_{\rm CORE}$$

$$F_K(r) = F_K(0) \times \left(\frac{r}{R_{\rm CORE}}\right)^{-1.8} \; ; \quad r > R_{\rm CORE} \; . \qquad (1)$$

The core radius for the cool stellar population is somewhat controversial but appears to lie in the range 15″–30″ (Rieke & Lebofsky 1987; Allen 1994; Rieke & Rieke 1994). Therefore, the innermost surface brightness is dominated by the blue stars.

SMBH Model A assumes that the CO-absorbing stars are completely absent inside a radius of $R_{\rm CO}$. Model B has a cool population extending into the core, with the number density of CO absorbing stars constant for $r < R_{\rm CO}$. SMBH prefered Model A because Model B requires the bluer population component to be added in such a way that the 2.2 μm light profile retains its $R^{-0.8}$ form into the core radius, which they felt was a contrived situation. It seems equally contrived that the cool population would be replaced by the hot one as in Model A while preserving the profile. In any case, the relatively lumpy profile from Figure 5 (below) renders arguments based on the smoothness of the brightness profile inconclusive.

Therefore, we have extended the models by considering the CO luminosity density to vary as

$$F_{\rm CO}(r) = F_K(R_{\rm CO}) \times \left(\frac{r}{R_{\rm CO}}\right)^{\alpha} \; ; \quad r \le R_{\rm CO}$$

$$F_{\rm CO}(r) = F_K(r) \; ; \qquad r > R_{\rm CO} \; , \qquad (2)$$

where $F_K(r)$ has the form given in equation (1). The value of the α parameter is important for interpreting the dispersions used in measuring the enclosed $M(r)$. If the stellar population inside $R_{\rm CO}$ is consistent with large α, the observed CO band depth at an apparent radius $r < R_{\rm CO}$ is dominated by stars at a true radius of $R_{\rm CO}$, and efforts to measure the enclosed mass versus radius will be meaningless within this region. However, if the CO depletion is such that $\alpha < 0$, the observed dispersion will be dominated by stars at the projected radius, even for $r < R_{\rm CO}$. The parameter values $\alpha = \infty$, $R_{\rm CO} = 10''$ and $\alpha = 0$, $R_{\rm CO} = 15''$ reproduce SMBH Models A and B, respectively.

Figure 4 shows the CO absorption for various values of α and $R_{\rm CO} = 10''$ compared to the observations. [For models with $\alpha < 0$, we set $F_{\rm CO}(r) = F_{\rm CO}(R_{\rm CORE})$ for $r < R_{\rm CORE}$, so that the number density of CO absorbers will remain bounded.] From Figures 3 and 4 together, the fits to the data favor intermediate parameter values, i.e., $\alpha \sim 1$, and $R_{\rm CO} \approx 8''$.

We can also constrain the behavior of the CO feature with our high-resolution imaging. In Figure 2, we have already removed the bright individual warm stars, for which Eckart et al. (1993) find a core radius of 3″.8. As shown in the figure, there may be a residual population of fainter stars with weak CO within ~3″ of Sgr A*. However, outside of a 6″ radius of Sgr

TABLE 5

ADDITIONAL CO VELOCITIES

Position	$\Delta\alpha$, $\Delta\delta$ Relative to Sgr A*	σ_v (km s^{-1})	V_{LSR} (km s^{-1})
P1 – 8[a]	−1.1, −2.5	110	−36
P1 – 9[a]	−1.1, −3.4	125	−42
P1 – 10[a]	−1.1, −4.2	104	−49
P1 – 16	−1.1, −9.4	79	−40
P2 – 5[a]	−3.1, 1.0	125	−105
P2 – 6[a]	−3.1, 0.2	150	−155
P2 – 7[a]	−3.1, −0.7	150	−167
P2 – 11[a]	−3.1, −4.1	150	20
P2 – 12[a]	−3.1, −5.0	0	45
P2 – 13[a]	−3.1, −5.9	150	−5
P2 – 14	−3.1, −6.7	125	67
P2 – 15	−3.1, −7.6	50	−80
P2 – 16	−3.1, −8.4	62	−80
P2 – 17	−3.1, −9.3	125	−30
P3 – 2[a]	3.9, 4.5	150	−55
P3 – 4	3.9, 2.8	125	−55
P3 – 9[a]	3.9, −1.5	100	−80
P3 – 10[a]	3.9, −2.4	150	20
P3 – 11[a]	3.9, −3.2	137	20
P3 – 12[a]	3.9, −4.1	150	−30
P3 – 13[a]	3.9, −4.9	350	−255
P3 – 16	3.9, −7.5	250	−280
P3 – 17	3.9, −8.4	250	−280
P7 – 5	0.4, 18.6	162	−30
P7 – 6	0.4, 17.8	150	20
P7 – 7	0.4, 16.9	200	45
P7 – 8	0.4, 16.1	200	70
P7 – 11	0.4, 13.5	175	7
P7 – 12	0.4, 12.6	125	7
P7 – 13	0.4, 11.8	50	−5
P7 – 14	0.4, 10.9	25	−5
P7 – 15	0.4, 10.1	75	−17
P7 – 16	0.4, 9.2	125	−30
P7 – 17	0.4, 8.3	100	−30
P7 – 18	0.4, 7.5	75	−92

[a] Radial distance from Sgr A* < 7″.

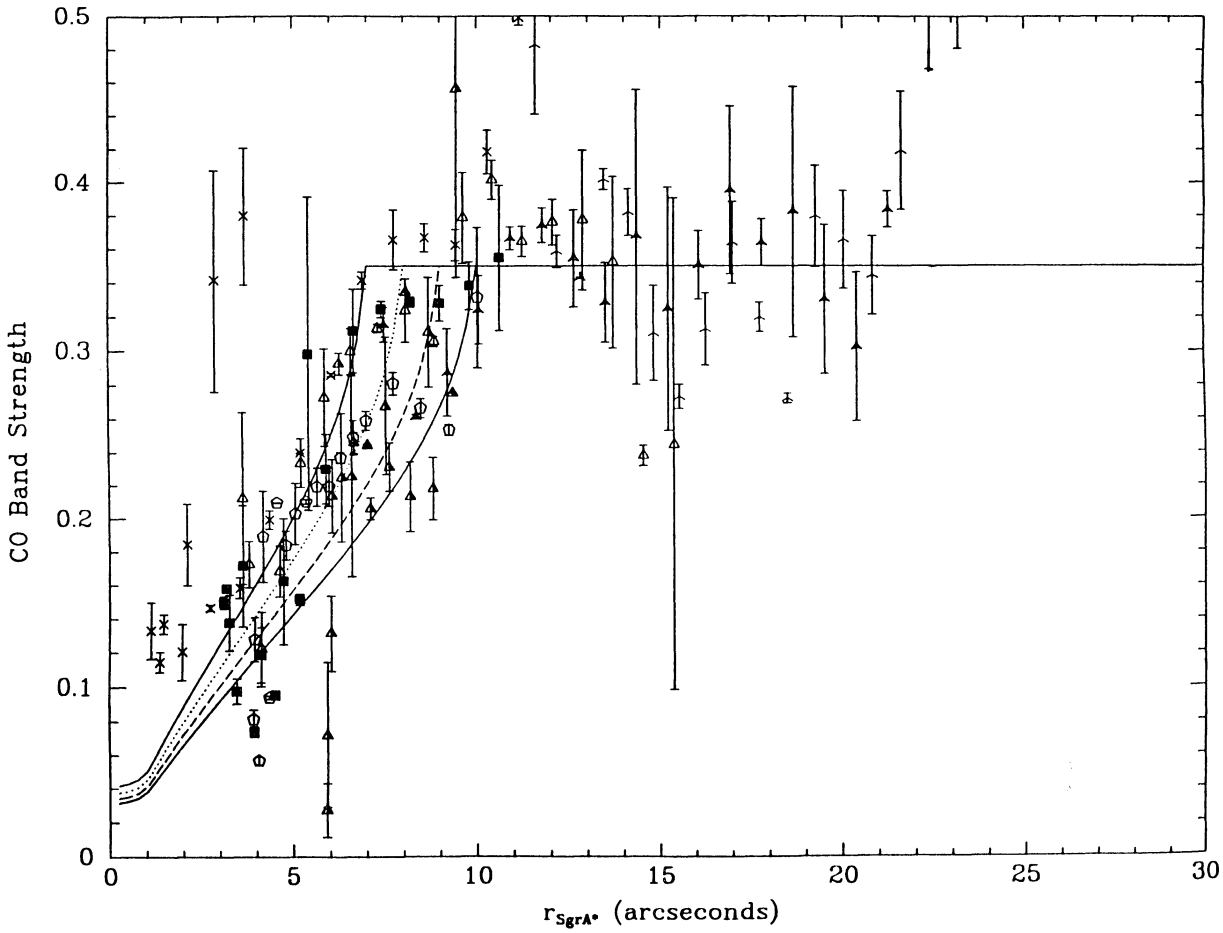

FIG. 3.—CO band strength from spectra vs. distance from Sgr A*. The modeled curves all assume an intrinsic CO band strength of 35% (at large distance from Sgr A*), with a velocity broadening correction of 20% (see text), and also $\alpha = \infty$. The curves correspond to $R_{CO} = 7''$, $8''$, $9''$, and $10''$ and suggest a best fit at $\sim 8''$.

A*, the CO band strength has reached a value that is typical for the entire region. This result is consistent with the modest reduction in the band depth we find between 10″ and 20″ in our spectra and the lower spatial resolution of the spectra compared with the images, particularly since the scatter in the spectrally determined CO depth appears to arise from the increasing number of contaminating blue sources and not necessarily from a reduction in the intrinsic CO depth.

We conclude that the CO-bearing stars may be useful mass tracers even close to Sgr A*. However, to be conservative, masses derived from these stars within a radius of 7″ should be considered as lower limits to the enclosed mass.

6. LIGHT DISTRIBUTION

A surface brightness profile for the Galactic center was derived from the large-scale K map. Before using this map, regions of high extinction were masked off. These regions consisted of the eastern to southeastern third of the map where a large molecular cloud covers much of our view, the molecular ring region, and an additional 1.4% of the area where the silhouettes of clouds were apparent. The surface brightness was measured in circular annuli centered on the position of Sgr A*; the annuli had a width of 0.″64 for $r < 15''$ and a width of 6.″4 for larger radii. Figure 5 shows the resulting curve compared to $r^{-0.8}$, which is a good fit from about 10″–200″.

The large-scale map photometry was also compared with the aperture photometry of Becklin & Neugebauer (1968). For this comparison the entire map was used regardless of extinction level. Fluxes were derived from apertures centered at 5″ south and 2″ east of IRS 7, and the flux of IRS 7 was subtracted from apertures which included it, in both cases in accordance with the approach of Becklin & Neugebauer. Figure 6 shows reasonable agreement between the new and old data. However, the $r^{-0.8}$ surface brightness distribution that was derived from the older data is in some measure fortuitous, with inclusion of regions of heavy extinction partially compensating possible beam cancellation in the largest apertures that reduced the flux levels. Nonetheless, outside the region of our large-scale image, the annular areas over which the surface brightness is measured are sufficiently large that the previous determinations of an $r^{-0.8}$ dependence of surface brightness should be valid. Combining with the result from our large-scale image, we therefore adopt an $r^{-0.8}$ surface brightness dependence for all regions outside the core radius.

7. DYNAMICS AND MASS OF THE GALACTIC CENTER

7.1. He I *Stars*

The He I–emitting stars represent a distinct tracer population confined largely to $r \leq 0.5$ pc from Sgr A*. Hence their velocities can be analyzed using the projected mass estimator (Bahcall & Tremaine 1981; Heisler, Tremaine, & Bahcall

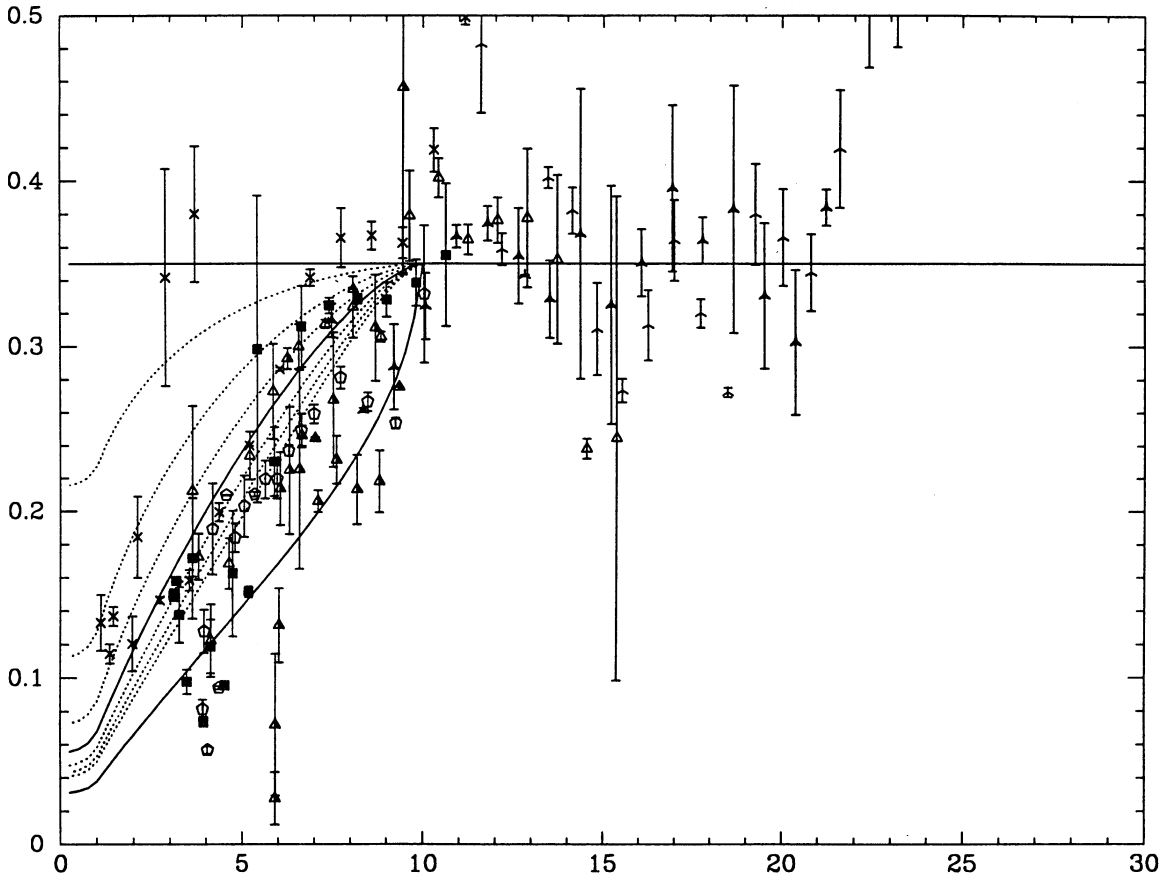

FIG. 4.—CO band strength. The models assume the core radius of the 2 μm light distribution to be 2.″5 and $R_{CO} = 10''$. The rightmost solid line is for $\alpha = \infty$; the next three dotted lines are, respectively, for $\alpha = +1.5$, $+1.0$, and $+0.5$; the other solid line is for $\alpha = 0$, and the next three dotted lines, respectively, for $\alpha = -0.5$, -1.0, and -1.5 (for these latter cases, a CO core radius has been imposed as explained in the text). Although the results are noisy, the best fit appears to require R_{CO} somewhat smaller than 10″ and α somewhat larger than 0.

1985). Use of this estimator on tracers that cannot be defined in a fashion that includes the outermost members tends to give an overestimate of the enclosed mass because the velocity dispersion of the population is overestimated if velocities for stars on eccentric orbits are based only on population members that are on the inner parts of their orbits (Haller & Melia 1995).

Using the projected mass estimator method, under the assumption of a dominant central mass and isotropic orbits, and accepting only the eight stars with He I line widths <200 km s^{-1}, we obtain an estimate of $1.8 \pm 0.9 \times 10^6\ M_\odot$. If we relax our line width criterion and include all 12 stars with He I widths <300 km s^{-1}, we find a mass of $2.3 \pm 0.9 \times 10^6\ M_\odot$. Both estimates apply to an average radius of $r \sim 0.25$ pc.

The search for He I stars is probably more complete near Sgr A* than in outlying regions, so some bias toward over-

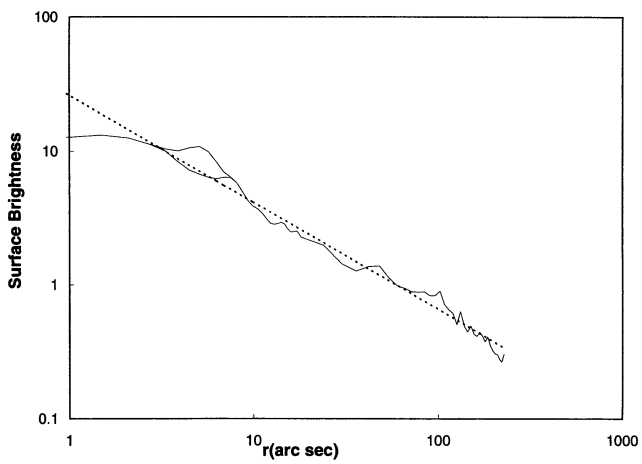

FIG. 5.—Surface brightness in mJy arcsec^2 plotted as a function of distance from Sgr A*. At $r \approx 7''$, two curves are shown with and without the contribution from IRS 7. The dashed line is an $r^{-0.8}$ distribution fitted between 15″ and 200″.

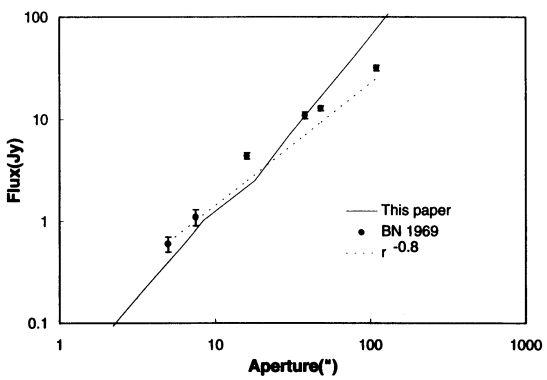

FIG. 6.—Enclosed flux as a function of aperture diameter. Data are from this paper and from Becklin & Neugebauer (1968). The dashed line is a fit of surface brightness $\propto r^{-0.8}$ to the Becklin & Neugebauer data.

estimation may still exist as discussed above. In addition, in § 4.1 we noted possible biases in the same direction due to wind velocities in these stars. In § 7.3 we discuss the possibility that the He I stars are on orbits that would result in our overestimating the enclosed mass. Therefore, these mass estimates must be interpreted as upper limits.

7.2. CO *Band Diffuse Emission*

McGinn et al. (1989) examined the CO band velocities of the diffuse stellar emission within 90″ of IRS 16. They used the Jeans equation for spherical systems (Hartwick & Sargent 1978) to estimate $2.5 \times 10^6\ M_\odot$ of material within 0.6 pc of IRS 16. Sellgren et al. (1990) extended this study to the central parsec. However, they concluded that the velocity dispersion measurements within 15″ (0.6) pc were really applicable to foreground and background stars and estimated $5.5 \pm 1.5 \times 10^6\ M_\odot$ of material within this radius. The uncertainty in the central mass could not be reduced significantly from the result of McGinn et al. because of the modeled behavior of the CO absorption.

Our more detailed modeling of the CO absorption suggests that we can safely make use of CO velocities if we interpret the estimated masses within a radius of 7″ from Sgr A* as lower limits. The enclosed mass distribution can be estimated from the observed velocity dispersion, $\sigma(r)$, rotational velocity, $V_{\rm ROT}(r)$, and light distibution by utilizing the Jeans equation (Hartwick & Sargent 1978; Sellgren et al. 1987; McGinn et al. 1989; Sellgren et al. 1990):

$$M(r) = \frac{r\sigma(r)^2}{G}\left[-\frac{d\ln n(r)}{d\ln r} - \frac{d\ln \sigma(r)^2}{d\ln r} + (\lambda - 2) + \frac{V_{\rm ROT}(r)^2}{\sigma(r)^2}\right]. \quad (3)$$

Here $n(r)$ is the number density of test particles, and λ is the ratio of the tangential to radial velocity dispersions. We have assumed isotropic stellar orbits ($\lambda = 2$). The run of $n(r)$ is derived from the 2.2 μm surface brightness distribution of the sample tracer population. At large distances from Sgr A*, the surface brightness falls as $r^{-0.8}$, leading to an assumed density falling as $r^{-1.8}$. However, the core radius for the CO-bearing stars is uncertain; we have considered the two extreme cases of 7″ and 30″ for this parameter. We have illustrated the uncertainities arising from the density law by considering both the case for an isothermal stellar distribution, and for a pseudo-isothermal core with an asymptotic $r^{-1.8}$ dependence. These two cases are illustrated in Figure 7.

The scatter in the velocities and dispersions from our measures of the "diffuse" CO emission, as well as from the previous measures of McGinn et al. (1989) and Sellgren et al. (1990), indicate that each beam position can be strongly influenced by a small number of relatively bright stars. We have therefore based our calculations on an average dispersion within a radial zone. To determine this dispersion, we converted the measured dispersion for each spectrum within the zone back to a Gaussian, shifted each Gaussian to $V_{\rm LSR}$ for that spectrum, and averaged with equal weight for each measurement.

An important geometric effect must be taken into account (Bicknell, Saha, & McGregor 1994; P. Saha, private communication), particularly if the core radius of the stellar distribution is large (e.g., 25″–30″). Within the core radius, projection effects are important in relating the observed radial velocity to the true rotation velocity at the apparent projected distance from Sgr A*. Failure to make the geometric corrections can result in significantly underestimated velocities as a function of true radius and hence an underestimate of the enclosed mass.

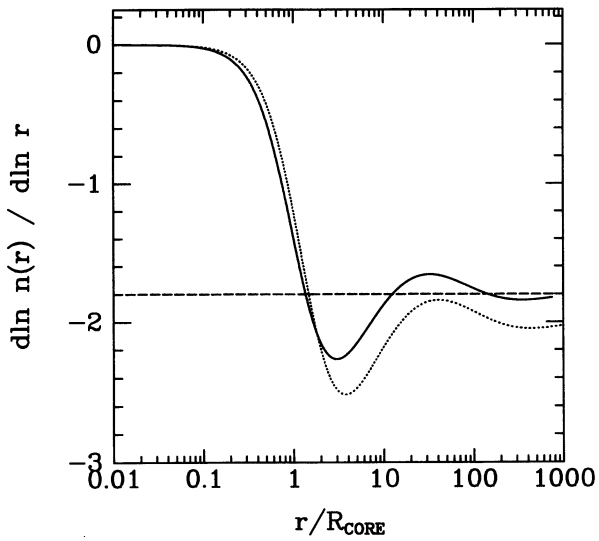

FIG. 7.—Comparison of the mass models used in our calculations. The solid line shows the logarithmic density gradient as a function of radius for a nonsingular isothermal model (as used by us). The dashed line shows the gradient for a singular isothermal model (as employed in some previous analyses). The dotted line shows the gradient for the pseudo-isothermal case that joins to the observational dependence (i.e., asymptotically behaves as $r^{-1.8}$).

Figure 8 shows the derived enclosed mass as a function of radius, assuming a core radius of 30″ (1.2 pc) and the pseudo-isothermal density distibution. A fit to the mass distribution is indicated; it assumes a point central mass of $1.8 \times 10^6\ M_\odot$ and an extended mass with a 30″ core radius and asymptotic $r^{-1.8}$ behavior at large distances. Figure 9 is similar, except the assumed core radius is 7″, and the assumed central point mass is $1.5 \times 10^6\ M_\odot$. It is important to note that using the correct projection geometry, as discussed in the preceding paragraph, has virtually removed any dependence of the best-fit central point mass on the core radius of the stellar distribution. Inside $r = 1$ pc, we also find that the derived mass is independent (to within a few percent) of the assumption of a pseudo-isothermal or isothermal core. This behavior arises because the velocity dispersion gradient dominates the density gradient within this region.

7.3. *Stellar Orbits*

The masses derived above from stellar dynamics are subject to uncertainties because of our lack of knowledge of the stellar orbits, which we have taken to be isotropic. Evidence that the stellar orbits are in fact isotropic comes from a comparison of $V_{\rm LSR}/\langle\sigma_v\rangle$ with the ellipticity of the isophotes of the stellar distribution (Kormendy & Illingworth 1982; McGinn et al. 1989), but complete justification can come only from isophotal and kinematic information on the diffuse emission for this region that is more detailed than is available. However, there is indirect supporting evidence in the form of comparisons of the enclosed masses from stellar dynamics with those calculated from well-measured gaseous features that appear to be in circular motion. We note in particular the close agreement

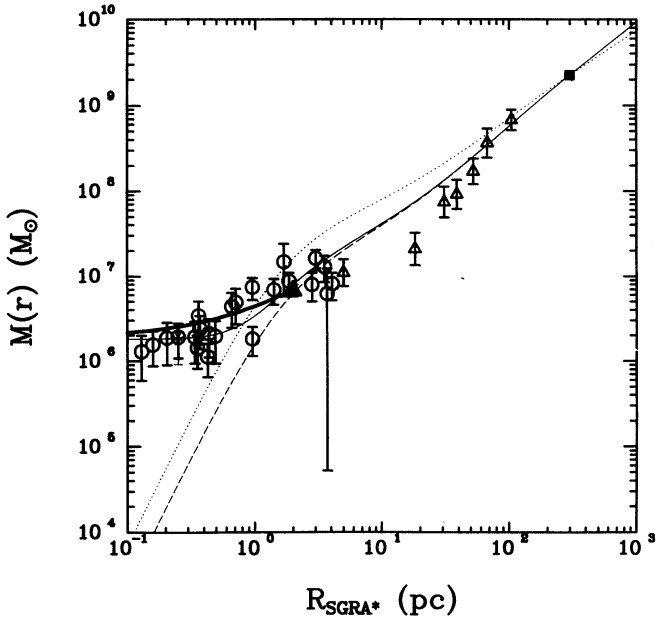

FIG. 8.—Enclosed mass distribution for central 300 pc. The core radius of the mass-bearing stars is taken to be 30″; the dashed line is for a pseudo-isothermal distribution, and the dotted one is for an isothermal one. The data points are as follows: filled box, Liszt & Burton (1978) and Burton & Liszt (1978); open triangles, Lindqvist et al. (1992); open circles, CO-bearing stars from this and previous works; filled triangle at 2 pc radius, molecular ring as estimated by Rieke & Rieke (1988); light cross at 0.25 pc radius, $1.8 \times 10^6 M_\odot$ (and lying under the CO points), He I stars from this work; and heavy line, fit to masses from [Ne II] measures, from Lacy et al. (1991). The light solid line is a fit assuming the mass is proportional to the light in the pseudo-isothermal stellar distribution, plus a central concentration of $1.8 \times 10^6 M_\odot$.

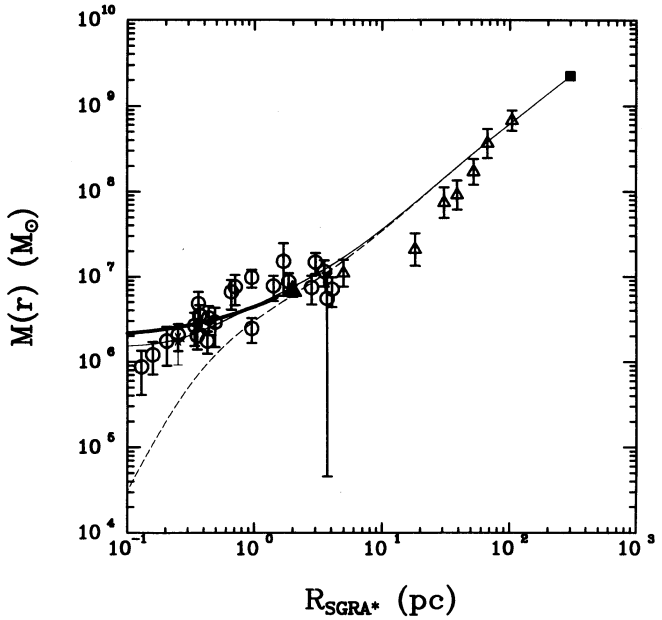

FIG. 9.—Same as Fig. 8, except the isothermal distribution is omitted, the core radius for the pseudo-isothermal distribution is taken to be 7″, and the fitted value of the central mass is $1.5 \times 10^6 M_\odot$.

between the calculated masses from stellar dynamics assuming isotropic orbits and those for the H I and CO gas and for the molecular ring (see Figs. 8 and 9 and discussion below). If we had normalized the stellar-determined masses to those from these gaseous features, our results would be unchanged.

As an additional control, we have examined whether there is a detectable change in stellar dynamics inside the parsec-scale molecular ring when compared with the dynamics outside this feature. We find no significant tendency for the rotation axis of the system to change inside the ring from its general orientation perpendicular to the Galactic plane. Although the dependence of rotation with distance from Sgr A* steepens within the central ~4 pc, there is no obvious change in this trend within 2 pc where it would invalidate our comparison. The smooth variation of the derived enclosed mass across the molecular ring also argues against a change occurring there.

However, we have no direct evidence that the He I stars have similar orbital parameters to the CO-bearing stars. The He I stars represent a very young population (Tamblyn et al. 1996) that is tightly confined around Sgr A* (Krabbe et al. 1991). They must have formed from gas that is confined in the gravitational potential of the Galactic center and that had presumably lost any highly noncircular components to its orbital motion. If so, then our assumption of isotropic orbits for the He I stars may result in an overestimate of the mass.

7.4. *Integration with Other Mass Determinations*

Figure 8 and 9 also summarize the mass distribution around the Galactic center on a large scale, combining the analysis in this paper with that of individual stellar velocities from Rieke & Rieke (1988), with that of the OH/IR stars by Lindqvist et al. (1992) and with measurements from well behaved gaseous features.

The analysis of the stellar velocities by Rieke & Rieke (1988) used the projected mass indicator without correction for the biases possible because of the finite sample volume and the lack of a unique tracer characteristic. Therefore, the values should be interpreted as upper limits to the enclosed mass. To place these measurements on a similar basis to those of the diffuse CO sources, we have converted them to velocity dispersions as shown in Table 6. We use the Jeans equation to calculate masses. The velocity dispersions from the individual stars are consistent with the dispersions from the diffuse emission; hence, the deduced masses are also similar.

Because of the biases implicit in use of the projected mass estimator with an incomplete population of test masses, we have shown the analysis of the data of Lindqvist et al. (1992) using the Jeans equation. They show that the projected mass indicator gives uniformly higher masses, as expected since it should return upper limits to the enclosed mass. We note that their data join smoothly onto ours and that the mass distribution appears to be well determined over a large region.

The parsec-scale molecular ring appears to be a roughly circular structure whose rotational velocity can therefore be taken to give a direct measure of the mass enclosed within it. Within a radius of 2 pc, Rieke & Rieke (1988) compute that the

TABLE 6

VELOCITY DISPERSIONS FROM INDIVIDUAL STELLAR VELOCITIES

Radial Range	Average Radius	Number of Stars	σ (km s^{-1})
7″–16″	10″	12	80 ± 8
16–30	23	9	61 ± 8
30–65	41	5	114 ± 33
65–135	105	10	51 ± 6

enclosed mass is $6.7 \pm 1.1 \times 10^6\ M_\odot$. An enclosed mass at 300 pc has been computed from the H I and CO data of Liszt & Burton (1978) and Burton & Liszt (1978).

The mass distribution deduced from the gas motions within the molecular ring has been measured with the [Ne II] emission line, as reported by Lacy et al. (1991). They also use the rotation of the molecular ring as a constraint on the total mass enclosed within ~ 2 pc. With this constraint, they derive an extended mass of $M_1 r$, with $M_1 = 2.5 \times 10^6\ M_\odot\ \mathrm{pc}^{-1}$ and a compact central mass of $1.9 \pm 0.5 \times 10^6\ M_\odot$. This distribution agrees excellently with our study of stellar dynamics, as shown in Figures 8 and 9. The close agreement strongly suggests that the mass distribution is correctly represented by these two approaches.

7.5. *Overall Distribution of Matter*

Given the good agreement, we can combine arguments from stellar dynamics and [Ne II] measurements to constrain the mass within the central ~ 0.2 pc. Both approaches suggest a lower limit of $1 \times 10^6\ M_\odot$ for this mass; this limit is most strongly established from the CO-bearing stellar dynamics, given the possibility that the gas motions might be affected by nongravitational forces. An upper limit of $3 \times 10^6\ M_\odot$ is provided by the [Ne II] measurements; a similar upper limit is also indicated by the He I stars. The existence of a $2 \times 10^6\ M_\odot$ central mass is placed on a far firmer basis than previously by this combination of limits.

In Figures 8 and 9, we also show the distribution of 2 μm light from relatively low luminosity stars as represented by the pseudo-isothermal models. The comparison of the light and mass distributions indicates a decrease in the ratio of $M/L_{2\ \mu\mathrm{m}}$ by a factor of about 2 between 100–300 pc and ~ 20 pc. This behavior is consistent with the presence of a relatively young stellar population in the central ~ 20 pc radius of the galaxy that could increase the 2 μm luminosity while contributing little mass. There is independent evidence for such a population from comparison of the stellar luminosity functions in Baade's window and in the central 10 pc (Haller, Rieke, & Rieke 1996) and from the change in properties of the OH/IR stars near 20 pc (Lindqvist et al. 1992). Within a radius of ~ 3 pc, however, M/L begins to rise. Because the relatively young population also lies within this region, the stellar M/L should be similar to that near 20 pc. Therefore, the rise in M/L may indicate the presence of an extended dark component within the central few pc in addition to a dark central mass.

7.6. *Nature of Dark Matter*

At least two types of dark matter can be expected to lie in the Galactic center. A central black hole has been widely anticipated, and the case by analogy to other galaxies has recently been strengthened by the demonstration of a strongly concentration mass of $\sim 2 \times 10^7\ M_\odot$ in the central parsec of NGC 4258 (Greenhill et al. 1995).

The second anticipated form of dark matter is stellar remnants. To estimate the mass that might be in this latter form, we can use a fit to the local initial mass function (Scalo 1986; Basu & Rana 1992) to approximate the IMF when stars first formed in the Galactic center. Normalized to $10^6\ M_\odot$, we then have

$$N(m)dm = 6.15 \times 10^5\ m^{-1.25}\ dm, \quad m \leq 0.56$$
$$= 2.65 \times 10^5\ m^{-2.7}\ dm, \quad m \geq 0.56\ , \qquad (4)$$

where the masses are in units of $M_\odot$ and we have taken the mass limits to be 0.05–120. To estimate crudely the stellar remnants produced by this population up to the present time, we take all stars with $m \geq 25$ to leave black hole remnants of $m = 10$ (Brown & Bethe 1994), all stars with $3 < m < 25$ to leave neutron star remnants with $m = 1.5$, and all stars with $0.7 < m \leq 3$ to leave white dwarf remnants of $m = 0.7$. It can then be shown that $\sim 23\%$ of the original mass would now be in the form of stellar remnants, $\sim 58\%$ would remain as low-mass stars, and $\sim 19\%$ would have been ejected as gas. More remnants will have been produced if the IMF is biased toward high-mass stars, as seems to be the case for some present-day starbursts (e.g., Rieke et al. 1993). That is, the ratio of mass in remnants to that in surviving stars is likely to be at least 0.4:1.

From these arguments, a mass in remnants of $\sim 2 \times 10^6\ M_\odot$ will have been produced in a volume with radius about 3 pc, if we take the stellar mass and multiply by the ratio of dark to stellar mass deduced from the IMF. The remnants would include approximately 2×10^6 white dwarfs, 2×10^5 neutron stars, and 5000 black holes. It appears that neutron stars are given a large dynamical "kick" at the time of formation, with a birth velocity of 450 ± 90 km s^{-1} (Lyne & Lorimer 1994); combined with the velocity dispersion of the parent stars, we expect a typical net velocity to be ~ 500 km s^{-1}. Consequently, they should form a dynamically hot population on highly elliptical orbits that take them well outside this region. However, particularly if they are concentrated by dynamical processes toward the center with moderate efficiency, the white dwarfs alone could account for a significant fraction of the dark matter in the region, including the extended dark matter which we infer might exist.

Morris (1993) has already suggested that remnants from the initial burst of star formation may provide substantial dark matter in the Galactic center. His work shows that, over the life of the Galaxy, remnants of mass ~ 1–$1.5\ M_\odot$ are likely to migrate inward by 1–2 pc from the sites of their formation. This estimate depends on the remnants not being given a large anomalous velocity at the time of their formation. Since the white dwarfs should retain the basic dynamics of their parent stars, the indicated degree of concentration could increase the portion of dark mass to stars from the ~ 0.4:1 ratio we estimated above to a value approaching 1:1.

Morris's estimate of the migration rate into the central 0.2 pc implies that sufficient concentration would not occur to account for the central $2 \times 10^6\ M_\odot$ in the same way. However, mass segregation can be greatly accelerated by time-dependent nonlinear effects. Lee (1995) has studied the behavior of $10\ M_\odot$ remnants under conditions appropriate to the Galactic center. He finds that the remnant population undergoes core collapse and becomes strongly concentrated in the central 0.1 pc radius; the embedding low-mass stellar population is only slightly affected in spatial distribution during this process. The timescale is strongly dependent on initial conditions.

The fate of the bulk of the dark mass, in the form of lower mass remnants, has not to our knowledge been studied at the same level of detail for conditions appropriate to a galactic nucleus. However, studies of globular clusters (e.g., Lee 1987) suggest that a postcollapsed core would achieve a segregation of remnants and stars that could account for the mass concentration in the Galactic center, even if the remnants are only slightly more massive ($\sim 1.3\ M_\odot$) than the stars. Phinney (1989) has shown that current estimates of the core radius in the Galactic center imply that it may have undergone core collapse.

7.7. *X-Ray Emission from Stellar Remnants*

Remnants in roughly the numbers calculated above must have been produced over the entire Galactic bulge. The expected emission from the resulting X-ray binaries and related phenomena can be reconciled with the observed flux, albeit with some difficulty (Fabbiano 1986; Rieke 1989). Within the central few parsecs, we must determine whether any additional X-ray emission associated with accretion of the gas confined in this region can increase this flux sufficiently to violate the observational upper limits.

We estimate the strength of this flux as follows. For nominal conditions in this region away from a potential accreting object, i.e., average particle density $n_\infty = 10^3$ cm^{-3}, gas temperature $T_\infty < 10^4$ K, and flow velocity $v_\infty \sim 500$ km s^{-1} (for neutron stars as discussed in the preceding section) or ~ 250 km s^{-1} (for white dwarfs or black holes), the average particle mean free path is $l_c \geq 6.7 \times 10^6$ cm. The stellar accretion radius (at which the particle kinetic energy = the potential energy) is $r_{acc} = 2GM/v_\infty^2$, for which $l_c/r_{acc} \leq 6 \times 10^{-5} \ll 1$. The gas therefore accretes hydrodynamically, with an accretion rate specified adequately by the Bondi (1952) theory as

$$\dot{M} = \frac{4\pi\tilde{\lambda}(GM)^2}{(a_\infty^2 + v_\infty^2)^{3/2}}\,\rho_\infty\,, \tag{5}$$

where a_∞ is the ambient sound speed, ρ_∞ is the ambient density, and $\tilde{\lambda}$ is a constant of order 1. The accretion flow is optically thin, since

$$\tau_{SC} \equiv \int_{R_*}^{\infty} \kappa_T\,\rho(r)dr \tag{6}$$

is $\tau_{SC}^{NS} \sim 6.7 \times 10^{-7}$ for neutron stars (with $R_* = 10$ km) and $\tau_{SC}^{BH} \sim 1.2 \times 10^{-6}$ for black holes (with $R_* = R_g = 2GM/c^2$, the Schwarzschild radius). Here, we have assumed that the gas is in free fall, and that it is mostly hydrogen for which $\kappa_T \approx 0.38$. Since the cyclotron/synchrotron emissivity at X-ray energies is negligible, the dominant emission mechanism is thermal bremsstrahlung, with a characteristic particle temperature $T(r)$, where $3kT(r) \approx GM(m_p + m_e)/r$.

In the case of neutron stars, most of the dissipated energy is radiated near the (hard) stellar surface, with a luminosity

$$L^{NS} \simeq \frac{GM\dot{M}}{R_*} \simeq 2.4 \times 10^{29}\ \text{ergs s}^{-1} \left(\frac{M}{M_\odot}\right)\left(\frac{\dot{M}}{1.8 \times 10^9\ \text{g s}^{-1}}\right). \tag{7}$$

From equation (7), the emission by white dwarfs (with $R_* \gg 10$ km) will be negligible compared with that from neutron stars. For black holes, most of the liberated energy is advected through the event horizon, under the assumption that no dissipation takes place in a disk. The black hole X-ray luminosity results primarily from emission at $r > R_g$:

$$L^{BH} \simeq \int_{R_g}^{\infty} \Lambda 4\pi r^2\,dr\,. \tag{8}$$

Here Λ is the (arbitrary relativistic) bremsstrahlung emissivity, and we have ignored gravitational and Doppler shifts for simplicity. For the same parameters as those quoted above, $L^{BH} \leq 1.8 \times 10^{20}$ ergs s^{-1}. Disk dissipation can increase the luminosity substantially, to

$$L_{disk}^{BH} \preceq \frac{1}{2}\frac{GM\dot{M}}{3R_g} \approx \frac{1}{2}\,L^{NS} \tag{9}$$

for the same M and $\dot{M}$ as in equation (7).

The average 3–150 keV luminosity seen by *Granat* from the inner $\sim 15'$ region is $L_{obs} \approx 2.5 \times 10^{36}$ ergs s^{-1} (Goldwurm et al. 1994). Since the high energy emission from this region is known to be variable over several years, L_{obs} can at most be an upper limit to the neutron star and black hole X-ray emission near the nucleus. In the case of neutron stars, this upper limit corresponds to a limit on the number of such objects, N^{NS};

$$N^{NS} \leq 10^7 \left(\frac{M}{M_\odot}\right)^{-3}\left(\frac{v_\infty}{500\ \text{km s}^{-1}}\right)^{3}\left(\frac{n_\infty}{10^3\ \text{cm}^{-3}}\right)^{-1}, \tag{10}$$

where M is the mass of the accreting remanant. For black holes $N^{BH} \leq 2N^{NS}$ if the accreting gas forms a disk at small radii. We have estimated that 2×10^5 neutron stars formed in the central 3 pc over the life of the galaxy; because of their highly ellipitical orbits, only a small fraction of this total would be within the region at only one time. Given the typical velocity for these objects of $v_\infty \sim 500$ km s^{-1}, this upper limit is satisfied easily. Similarly, the X-rays from white dwarfs are of little concern because of the low luminosity per object, and from black holes because of the small number of objects. Therefore, the X-ray flux from this region is consistent with a total mass of a few times $10^6\ M_\odot$ in stellar remnants within the central few parsecs.

Thus, the data suggest that the central $6 \times 10^6\ M_\odot$ of the Milky Way may be roughly equally divided among a compact central mass, stars, and an extended distribution of stellar remnants. Although a black hole remains the most plausible explanation for the compact central $2 \times 10^6\ M_\odot$, it is not yet possible to exclude alternate explanations such as a compact cluster of stellar remnants. An improved understanding of the stellar distribution in the region may help test this alternate possibility, since the formation of such a central cluster would probably require the stellar distribution to have undergone core collapse.

8. CONCLUSIONS

We report an extensive new set of velocity measurements of CO- and He I–bearing stars in the Galactic center. These measures are analyzed to show the following:

1. The stellar dynamics place strong limits on the mass of a concentrated central object, which must lie between 1 and $3.6 \times 10^6\ M_\odot$.
2. The mass deduced from stellar dynamics is in close agreement with that from gas velocities measured in the [Ne II] line.
3. In addition to the central mass, the presence of an extended distribution of dark matter can be inferred. It is potentially of comparable mass within the central 3 pc to the stars and also to the central object.
4. Future studies need to address the role of stellar remnants in both the extended and compact components of dark mass.

We appreciate helpful discussions with A. Burrows, O. Gerhard, J. Kormendy, J. Lacy, H. M. Lee, and P. Saha. The staffs of CTIO, the MMTO, and the SO 90 inch assisted us in many ways to obtain these observations. This work was supported by NSF under AST 91-16442 and NASA under NAGW-2822.

REFERENCES

Allen, D. K. 1994, in Nuclei of Normal Galaxies—Lessons from the Galactic Center, ed. R. Genzel & A. Harris (Dordrecht: Kluwer), 293
Allen, D. K., Hyland, A. R., Hillier, D. J., & Bailey, J. A. 1989, in IAU Symp. 136, The Center of the Galaxy, ed. M. Morris (Dordrecht: Kluwer), 513
Bahcall, J. N., & Tremaine, S. 1981, ApJ, 244, 805
Basu, W., & Rana, N. C. 1992, ApJ, 219, 1008
Becklin, E. E., & Neugebauer, G. 1968, ApJ, 151, 145
Bicknell, G. V., Saha, P., & McGregor, P. J. 1994, BAAS, 24, 1478
Bondi, H. 1952, MNRAS, 112, 195
Brown, G. E., & Bethe, H. A. 1994, ApJ, 423, 659
Burton, W. B., & Liszt, H. S. 1978, ApJ, 225, 815
Close, L. M., & McCarthy, D. W. 1994, PASP, 106, 27
Eckart, A., Genzel, R., Hofmann, R., Sams, B. J., and Tacconi-Garman, L. E. 1993, ApJ, 407, L77
Fabbiano, G. 1986, PASP, 98, 525
Genzel, R., & Townes, C. H. 1987, ARA&A, 25, 377
Goldwurm, A., et al. 1994, Nature, 371, 589
Greenhill, L. J., Jiang, D. R., Moran, J. M., Reid, M. J., Lo, K. Y., & Claussen, M. J. 1995, ApJ, 440, 619
Hall, D. N. B., Kleinmann, S. G., & Scoville, N. Z. 1982, ApJ, 260, L53
Haller, J., & Melia, F. 1995, ApJ, submitted
Haller, J., Rieke, M. J., & Rieke, G. H. 1996, in preparation
Hartwick, F. D. A., & Sargent, W. L. W. 1978, ApJ., 221, 512
Heisler, J., Tremaine, S., & Bahcall, J. N. 1985, ApJ, 298, 8
Kormendy, J., & Illingworth, G. 1982, ApJ, 256, 460
Krabbe, A., Genzel, R., Drapatz, S., & Rotaciuc, V. 1991, ApJ, 382, L19
Lacy, J. H. 1989, in IAU Symp. 136, The Center of the Galaxy, ed. M. Morris (Dordrecht: Kluwer), 493
Lacy, J. H., Achtermann, J. M., & Serabyn, E. 1991, ApJ, 380, L71
Lacy, J. H., Townes, C. H., Geballe, T. R., & Hollenbach, D. J. 1980, ApJ, 241, 132
Lee, H. M. 1987, ApJ, 319, 772
———. 1995, MNRAS, 272, 605
Lindqvist, M., Habing, H. J., & Winnberg, A. 1992, A&A, 259, 118
Liszt, H. S., & Burton, W. B. 1978, ApJ, 226, 790
Lyne, A. G., & Lorimer, D. R. 1994, Nature, 369, 127
McGinn, M. T., Sellgren, K., Becklin, E. E., & Hall, D. N. B. 1989, ApJ, 338, 824
Morris, M. 1993, ApJ, 408, 496
Phinney, E. S. 1989, in IAU Symp. 136, The Center of the Galaxy, ed. M. Morris (Dordrecht: Kluwer), 543
Rieke, G. H. 1989, in IAU Symp. 136, The Center of the Galaxy, ed. M. Morris (Dordecht: Kluwer), 21
Rieke, G. H., & Lebofsky, M. J. 1987, In AIP Conf. Proc. 155, The Galactic Center, ed. D. Backer (New York: AIP), 91
Rieke, G. H., Loken, K., Rieke, M. J., & Tamblyn, P. 1993, ApJ, 412, 99
Rieke, M. J., Rieke, G. H., Green, E. M., Montgomery, E. F., & Thompson, C. L. 1993, Proc. SPIE, 1946, 179
———. 1994, in Nuclei of Normal Galaxies—Lessons from the Galactic Center, ed. R. Genzel & A. Harris (Dordrecht: Kluwer), 283
Rieke, G. H., & Rieke, M. J. 1988, ApJ, 330, L33
Rieke, G. H., Rieke, M. J., & Paul, A. E. 1989, ApJ, 336, 752
Scalo, J. M. 1986, Fundam. Cosmic Phys., 11, 1
Sellgren, K., Hall, D. N. B., Kleinmann, S. G., & Scoville, N. Z. 1987, ApJ, 371, 881
Sellgren, K., McGinn, M. T., Becklin, E. E., & Hall, D. N. B. 1990, ApJ, 359, 112 (SMBH)
Tamblyn, P., Rieke, G. H., Hanson, M. M., Close, L., McCarthy, D. M., & Rieke, M. J. 1996, ApJ, 456, 206
Williams, D. M., Rieke, G. H., Thompson, C. L., & Montgomery, E. F. 1993, Proc. SPIE, 1946, 482
Wollman, E. R., Smith, H. A., & Larson, H. P. 1982, ApJ, 258, 506